Danmarks Tekniske Universitet

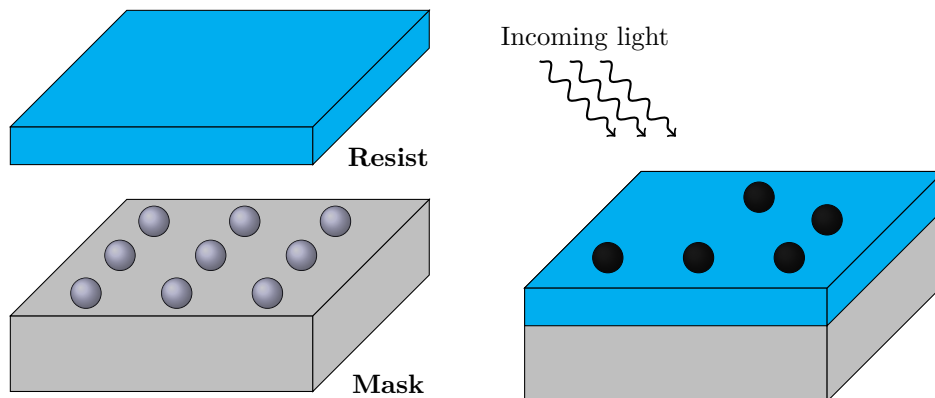DTU

34029 Physics Project

Programmable Nanolithography

Authors:
Emil Duegaard (s123517)
Nikolaj Knøsgaard (s123406)
Andreas Kristensen (s123056)

Supervisors:
Jakob R. de Lasson
Anders Nysteen
Phillip T. Kristensen
Jesper Mørk

January 15, 2014

Abstract

The purpose of the study was to investigate the possibility of using spherical silver particles arranged in an array to create different imprints in photoresist for use in photolithography. A masking pattern can be generated by illuminating the particles with a plane wave at some incident angle and polarisation. The paper was based on the work done by Koenderink et al. [1] whose results show that it is possible to create an imprint, however the research done in this paper contradicts their findings. By using MATLAB simulations we obtained results that show it is possible to create a pattern by illuminating the particles, but not to an extend that Koenderink et al. suggests. The paper introduces wave calculations in one dimension originating from Maxwell's equations, followed by the development of a MATLAB script able to compute a wave travelling in different media. As a prelude to the three dimensional calculations the volume integral equation is introduced and solved using Green's function in one dimension to generalize the solution. In the end the paper delves into the question of how realistically a silver particle mask would be achieved. First of all the findings suggest that it would be near impossible to arrange the particles in an array and secondly hard to find a photoresist designed for the intensity of the dissipated power of the silver spheres.

Contents

List of Figures

Introduction

The article "Programmable Nanolithography with Plasmon Nanoparticle Arrays" by A. Femius Koenderink et al. describes how a new technique can be used to create different patterns used in nanolithography. According to the team, this can be achieved by changing the wavelength and polarization of the incidental light. With the use of an approximative point dipole model, the team explores the local response of silver particles in small two-dimensional arrays of 50-200 nm spacing.

With this idea the world of micro- and nanofabrication would be significantly improved due to a an increased resolution of photolithography.

In this paper we will try to recreate the results presented in the article. We will start by describing some of the important concepts in the article.

1.1   Review of concepts

One of the most widely used techniques in fabrication of micro- and nanostructures is photolithography. It is a process used to print different patterns in a substrate (called a wafer) which requires a large number of procedures such as cleaning, preparation, etching etc. These techniques are mostly used in industrial semiconductor processing but recently they have proved helpful in the progress of nanoscience.

In the process of making a wafer a procedure is to add photoresist to the substrate. A photoresist is a material which is sensible to light changing chemical properties when exposed. In regards to the article this means you can create different patterns depending on how the substrate with particles is exposed.

Photolithography relies on far-field imaging. This means that the light we send towards the substrate can be seen as plane waves. Photolithography is therefore limited by the diffraction limit which means that resolution of the pattern depends on wavelength.

To surpass the diffraction limit to create even smaller structures we can use a near-field technique involving surface plasmons interference. Surface plasmons

are in short a collective of electron oscillations which can alter an electric field.

1.2   Article

Before we get into the physics behind this technique we will describe in a more detailed way which problems they are trying to solve in the article by Koenderink et al. [1].

Three particles are placed in a line array (figure 1.1) which is embedded on a transparent mask (the refractive index, n = 1.5) and a photoresist is deposited on the mask. The team uses a point-dipole model to approximate the field as constant within the spheres. By tuning the angle of the incoming light the team creates different patterns.
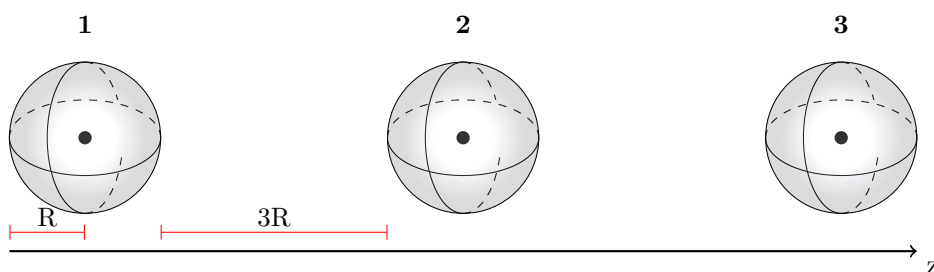
Figure 1.1 We consider three silver particles in an array with radius 25 nm and distance to the nearest is 75 nm.

The reason why they use these particles is because of the plasmon effect at the surface on a silver nanoparticle. The plasmon resonance at the surface of a silver particle have an ability to enhance the electric field intensities at visible wavelengths. One silver nanoparticle has a radius of 25 nm and the distance between two particles is 75 nm because with this radius and distance the contrast to the next brightest sphere will be highest. This is illustrated on the graph in figure 1.2(B) where they have plotted the contrast of the end sphere relative to next brightest sphere as a function of particle spacing for several particle radii in order to determine which particle spacing and radius will be the optimal. The simulations shows that the contrast to the next brightest sphere will be highest with the use of a particle with a radius of 25 nm and spacing 75 nm. But it shows that spacing particles in the range from 25 to 150 nm is also appropriate.

If we again consider the setup where we have three silver nanoparticles in a linear array. We are able to send unfocused light towards the mask and create different patterns depending on the incident angle. For instance if we want to let the silver particle in the middle be the one with the highest intensity, how would we be able to accomplish that? The results from the article show that if we send light perpendicular to the mask the sphere in the middle will get the highest intensity. But if we instead send light from one of the ends the opposite sphere will have the highest intensity. That does not
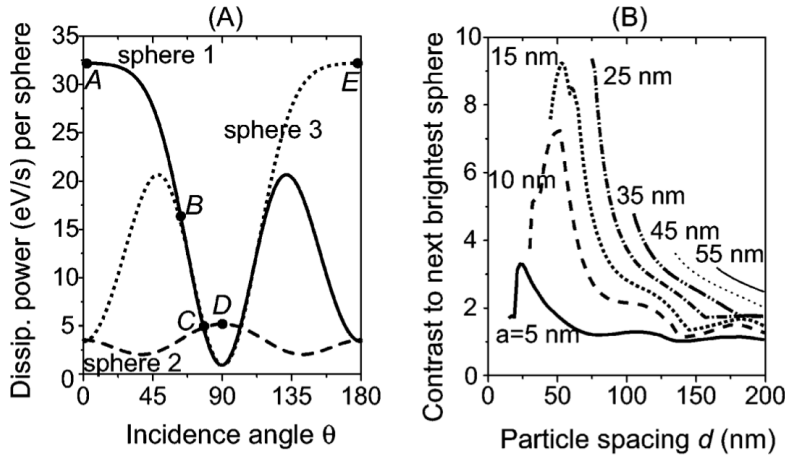
Figure 1.2 In (A) we see the dissipated power per sphere as a function of the incidence angle. Notice the contrast at points A/E and D are remarkably high corresponding to one sphere exposed either in left/right or in the middle. The graphs in (B) shows different radii of silver particles labeled with *a*. As we can see on this graph it makes sense why they have chosen to use a particle with a radius of 25 nm and a particle distance of 75 nm because this is where the contrast to the next brightest sphere is highest within the limits of their point-dipole model. These two graphs are taken directly from the article [1].

make sense. Why would the particle that is placed farthest from the light at this angle be the one with highest intensity? To answer this question we need to look at the aforementioned surface plasmons of the silver particles. Somehow created destructive interference between the two spheres nearest the light and constructive interference between the last one and the one in the middle happens. This example is also shown in figure 1.2(A) where we see a plot of the dissipated power per sphere as a function of the incidence angle.

The same simulation is made for 2×2 -array of particles and finally for 3×3 -array of particles. The 3×3 -configuration is illustrated in figure 1.3 where the experiment as a whole is sketched before and after depositing the photoresist.

1.3 Motivation

In this paper we will seek to recreate the results presented in the article through simulations with the software MATLAB. This will lead us to our main goal which is to approve or disapprove the findings stated in the article, that is to determine if it is possible or not to create the patterns in the photoresist.

In the next chapter we will start by solving Maxwell's equations for electromagnetic waves in one dimension using boundary conditions. We will develop a MATLAB function which can be used to specify a desired configuration of refractive indices representing different matter and analyse how light by chosen wavelengths and intensity levels propagate through the configuration. We will

(a) Silver particles placed on mask   **(b)** An example of a pattern
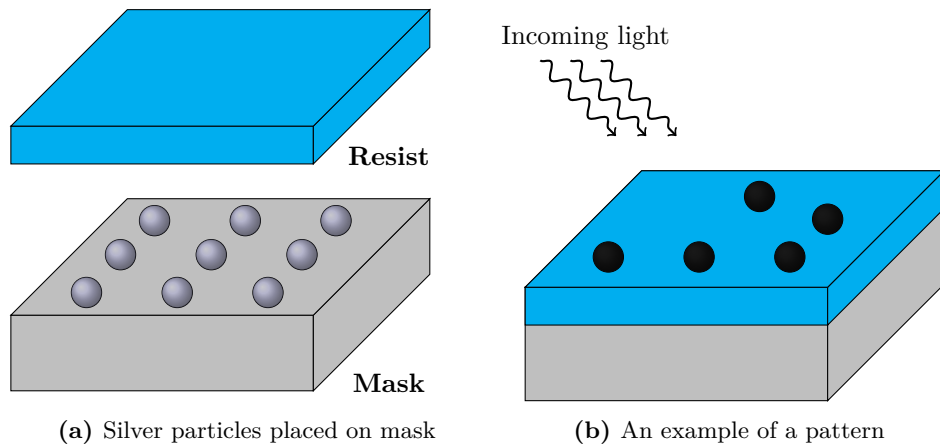
Figure 1.3 Configuration of the experiment where 3×3 silver particles is embedded on a transparent mask with refractive index 1.5. Each particle has a radius of 25 nm and the distance between them are 75 nm. A layer of photoresist is added on top of the mask. The black areas on (b) are an example of pattern created. These different patterns depends on wavelength, polarization, and incidence angle of the incoming light.

furthermore take a look into the application of our function and see it used in a physical problem concerning Fiber Bragg gratings.

In chapter 3 we will solve Maxwell's equations yet again, but this time by using Green's functions. We will introduce the volume integral eqaution and solve this with the help of Green's functions. This is to get a more general solution and will make it easier to migrate to the three dimensional problem.

In chapter 4 we will use a MATLAB function developed by J.R. de Lasson to simulate the problem in three dimensions and compare our results with the results from the article.

Hereafter we will discuss the problems of an actual practical application using a top-down approach. For instance which properties the photoresist must contain in order to make any of this happen. Finally, we will sum up the paper and link our conclusion to the main goal.

One-dimensional wave interactions

2.1 Maxwell's equations

When looking at how light interfers with media, Maxwell's equations are central because they are the foundation of classical electrodynamics (together with the Lorentz force law) and therefore describes exactly how light behaves. We use two of the four equations, that is Faraday's law and Ampere's law concerning the rotation of the electric and magnetic field: [2]

$$\boldsymbol{\nabla} \times \mathbf{E} = -\frac{\partial \mathbf{B}}{\partial t} \tag{2.1}$$

and

$$\boldsymbol{\nabla} \times \mathbf{H} = \frac{\partial \mathbf{D}}{\partial t}. \tag{2.2}$$

Together with Gauss's laws for electrostatics and magnetics they form the set of four Maxwell equations. Here $\mathbf{E}$ is the electric field, $\mathbf{B}$ is the magnetic field, $\mathbf{H}$ is the auxiliary field and $\mathbf{D}$ is the electric displacement field.

The electric displacement is given by $\mathbf{D} = \epsilon_0 \mathbf{E} + \mathbf{P}$, and if the media is linear the polarization, $\mathbf{P}$, is given by $\mathbf{P} = \epsilon_0 \chi_e \mathbf{E}$

$$\begin{aligned} \mathbf{D} &= \epsilon_0 \mathbf{E} + \epsilon_0 \chi_e \mathbf{E} \\ &= \epsilon_0 \left(1 + \chi_e\right) \mathbf{E} \\ &= \epsilon_0 \epsilon_r \mathbf{E} \\ &= \epsilon \mathbf{E}. \end{aligned} \tag{2.3}$$

Here $\epsilon_r = 1 + \chi_e$ is the relative permittivity, ϵ_0 is the permittivity of free space and $\epsilon = \epsilon_0 \epsilon_r$ is the permittivity. χ_e is the eletric susceptibility. For linear media we also have that $\mathbf{B}$ is proportional to $\mathbf{H}$ by the proportionality factor μ called the permeability.

$$\mathbf{B} = \mu \mathbf{H}. \tag{2.4}$$

The electromagnetic functions, $\mathbf{E}$ and $\mathbf{H}$, depends on both time and frequency and therefore we split them into a time domain and a frequency domain:

$$\mathbf{E}(\mathbf{r}, t) = \mathbf{E}(\mathbf{r}, \omega) \exp(-i\omega t) \tag{2.5}$$

$$\mathbf{H}(\mathbf{r}, t) = \mathbf{H}(\mathbf{r}, \omega) \exp(-i\omega t). \tag{2.6}$$

By using (2.5) and (2.6), (2.1) now gives

$$\begin{aligned}
\boldsymbol{\nabla} \times \mathbf{E}(\mathbf{r}, t) &= -\frac{\partial}{\partial t} \left(\mu \mathbf{H}(\mathbf{r}, \omega) \exp(-i\omega t) \right) \\
&= i\omega\mu\mathbf{H}(\mathbf{r}, \omega) \exp(-i\omega t) \\
&= i\omega\mu\mathbf{H}(\mathbf{r}, t),
\end{aligned} \tag{2.7}$$

and (2.2) gives:

$$\boldsymbol{\nabla} \times \mathbf{H}(\mathbf{r}, t) = -i\omega\epsilon\mathbf{E}(\mathbf{r}, t). \tag{2.8}$$

Because of the harmonic time variability (complex exponential functions) the time dependence cancels out of the equations and gives us the simplified expressions:

$$\boldsymbol{\nabla} \times \mathbf{E} = i\omega\mu\mathbf{H}, \tag{2.9}$$

and

$$\boldsymbol{\nabla} \times \mathbf{H} = -i\omega\epsilon\mathbf{E}. \tag{2.10}$$

At this state we have two coupled differential equations. To de-couple them the order of differentation is raised by taking the rotation on both sides:

$$\begin{aligned}
\boldsymbol{\nabla} \times \boldsymbol{\nabla} \times \mathbf{E} &= \boldsymbol{\nabla} \times (i\omega\mu\mathbf{H}) \\
&= i\omega\mu\boldsymbol{\nabla} \times \mathbf{H} \\
&= i\omega\mu(-i\omega\epsilon\mathbf{E}) \\
&= \omega^2\mu\epsilon\mathbf{E},
\end{aligned} \tag{2.11}$$

and

$$\boldsymbol{\nabla} \times \boldsymbol{\nabla} \times \mathbf{H} = \omega^2\mu\epsilon\mathbf{H}. \tag{2.12}$$

For the $\mathbf{E}$-field the expression $\boldsymbol{\nabla} \times \boldsymbol{\nabla} \times \mathbf{E} = k_0^2\epsilon_r\mathbf{E}$ will be used where $k_0^2 = \dfrac{\omega^2}{c^2}$ and $c = \dfrac{1}{\sqrt{\epsilon_0\mu}}$. This is the general three-dimensional wave equation for the electric field. We will use this equation to look at a more simple one-dimensional example.

In one dimension we assume that the electric field propagates in one direction with a polarization in another direction, for example $\mathbf{E} = E_x(z)\hat{\boldsymbol{x}}$. Here $\hat{\boldsymbol{x}}$ is the polarization direction and $\hat{\boldsymbol{z}}$ is the direction of propagation. That results in $\boldsymbol{\nabla} \times \mathbf{E} = \partial_z E_x\hat{\boldsymbol{y}}$ and $\boldsymbol{\nabla} \times \boldsymbol{\nabla} \times \mathbf{E} = -\partial_z\partial_z E_x\hat{\boldsymbol{x}}$. The differential equation for $\mathbf{E}$ in one dimension therefore is

$$\begin{aligned}
\frac{\partial^2}{\partial z^2} E_x(z) + k_0^2\epsilon_r E_x(z) &= 0 \\
\frac{\partial^2}{\partial z^2} E_x(z) + k^2 E_x(z) &= 0,
\end{aligned} \tag{2.13}$$

where

$$k^2 = k_0^2 \epsilon_r = k_0^2 n^2 \Leftrightarrow k = k_0 n.$$

Here the refractive index n is given as $n = \sqrt{\epsilon_r}$.

The homogeneous differential equation (2.13) has solutions in form of

$$E_x(z) = A \exp(ikz) + B \exp(-ikz), \qquad A, B \in \mathbb{C}. \qquad (2.14)$$

2.2 Wave interaction with a single interface

With the equations obtained in (2.14) we can solve the wave equation for a single interface by considering appropriate boundary conditions.

Referring to figure 2.1 we assume that the wave must be continuous thus the waves in each domain 1 and 2 and their derivatives must be equal over the interface. The situation is sketched in figure 2.1, where A_I, B_R and A_T are the complex amplitudes of the incoming wave, reflected and transmitted wave respectively.
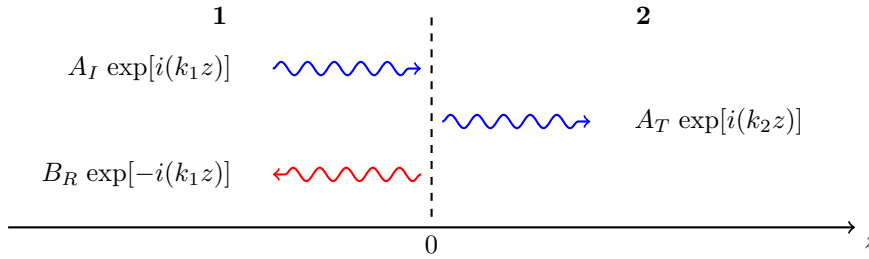
Figure 2.1 A wave travelling in the direction of the z-axis reaching an interface situated at $z = 0$, where a part of the wave is reflected and another transmitted in the domains 1 and 2.

The assumption yields:

$$A_I \exp(ik_1 z) + B_R \exp(-ik_1 z) = A_T \exp(ik_2 z)$$
$$ik_1 A_I \exp(ik_1 z) + -ik_1 B_R \exp(-ik_1 z) = ik_2 A_T \exp(ik_2 z).$$

Which can be solved when $z = 0$ as figure 2.1 imply.

$$A_I + B_R = A_T \qquad (2.15)$$
$$k_1 A_I - k_1 B_R = k_2 A_T. \qquad (2.16)$$

Substitute (2.15) into (2.16) solving for A_R then substituting the result back into (2.15) yields:

$$B_R = A_I \frac{k_1 - k_2}{k_2 + k_1} \tag{2.17}$$

$$A_T = A_I \left(1 + \frac{k_1 - k_2}{k_2 + k_1} \right). \tag{2.18}$$

By examining the result it is seen that $B_R \to -A_I$ and $A_T \to 0$ as $k_2 \to \infty$ which equals that the refractive index of the second domain becomes much greater than that of the first domain: $n_2 >> n_1$ when $k = k_0 n$ and $k_0 = \frac{2\pi}{\lambda_0}$. In this situation all of the incoming light will be reflected and none will be transmitted.

In the case $k_2 \to k_1$ it is seen that $B_R \to 0$ and $A_T \to A_I$ which of course shows that two materials with the same refractive indices inherit the same optical attributes. The coefficients B_R and A_T calculated here are commonly known as the Fresnel coefficients for a single interface with incoming light perpendicular to the interface.

We can conclude that a surface will act as a mirror and increase reflectivity when the refractive index becomes larger than that of the current material the wave is travelling through.

2.3   Wave interaction with p-interfaces

We will now expand the model to include any p numbers of interfaces. This produces a so called "landscape" of varying refractive indices which could look like something sketched in figure 2.2a.

To solve this problem with regards to boundary conditions, we must once more assume that the wave must be continuous, so the wave and it's derivatives are equal over each interface. Equation (2.14) can be solved for each interface where the complex amplitude A describes transmitted light and B describes reflected light.

We found a convenient way to solve the p-interface problem by using linear algebra. A matrix containing the equations outlined by boundary conditions can be written systematically, which gives a matrix equation on the following form: $\boldsymbol{Mx} = \boldsymbol{c}$, where $\boldsymbol{M}$ has the size of $2p \times 2p$ and contains the coefficients of the unknown amplitudes in $\boldsymbol{x}$, $\boldsymbol{c}$ constitutes the right-hand side and will contain our known factors: the amplitude of the incoming light and the position of the interface. This equation can be solved by ordinary means to determine the coefficients of reflected and transmitted light on each side of the interface. As an example we can take a look at a landscape $p = 3$ interfaces shown on figure 2.2b. This generates matrices that can be written on a form for arbitrary refractive indices and interface positions which can be seen in appendix A.

In the matrix k_a denotes the refractive index in the area given by an external vector containing the refractive indices of the landscape and z_p points to the location of the interface. In general $a = p + 1$ because the first element refers

to the refractive index on the left of the first interface, i.e. the first domain of the landscape.

When we know the overall layout of the matrices we can create a MATLAB function which enables us to simulate a wave through a landscape consisting of any combination of discrete refractive indices by passing it as an argument to the function. It is passed as two vectors: the first containing refractive indices with a total of a areas and a second containing the specific locations of the interfaces $p = a - 1$ as previously stated.

The matrix, $\boldsymbol{M}$, is then created by manually changing the values in the appropriate spots for the first and last interface. The rest of the interfaces ($p - 2$) are constructed and added by using a loop.

To test our code to see whether or not it is working, it is natural to compare it to the analytical equations for reflection and transmission of a wave incident to a single interface derived in equation (2.17) and (2.18).

We choose the wavelength of the incoming light to 633 nm and the amplitude to 1. For the function we pass the index landscape as $[n_1 \ n_2 \ n_2]$ with a spacing of 500 nm between each interface. We extract numerically calculated coefficients of transmitted and reflected light sweeping over values of $n_1 = 1$ and $n_2 = [1.1, 4]$. We calculate the analytical values for reflection and transmission coefficients using (2.17) and (2.18). The relative deviation between the analytical and numerical values are calculated and the result is plotted versus n_2. We obtain a plot as shown on figure 2.3 where it is seen that the numerical deviation equals that of the range of MATLAB when it saves data as double precision floating-point numbers [3]. If we take a closer look at the expressions: $\frac{|r_n - r_a|}{|r_a|}$ and $\frac{|t_n - t_a|}{|t_a|}$ for $n_2 \rightarrow n_1$ we get that $r_n \rightarrow 0$, $r_a \rightarrow 0$, $t_n \rightarrow 1$ and $t_a \rightarrow 1$. This causes $\frac{|r_n - r_a|}{|r_a|} \rightarrow \infty$ and $\frac{|t_n - t_a|}{|t_a|} \rightarrow 0$ explaining the tendency in the distribution of deviation pictured in the figure. With the result being within the error margin of MATLAB the numerical result is virtually the same as the analytical which enables us to conclude that our code is functioning.

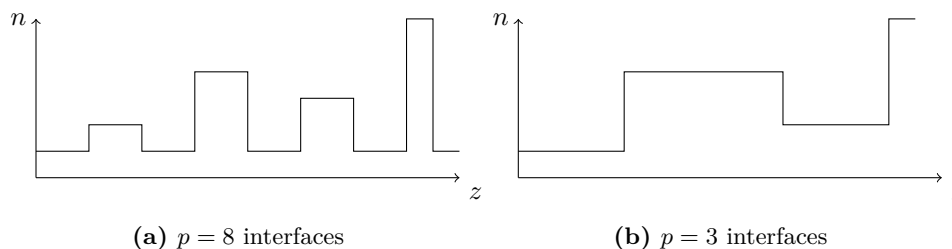(a) $p = 8$ interfaces   (b) $p = 3$ interfaces

Figure 2.2 A potential landscape of varying refractive indices, in the setup to the left there is a total of $p = 8$ interfaces in the setup to the right there is a total of $p = 3$ interfaces.
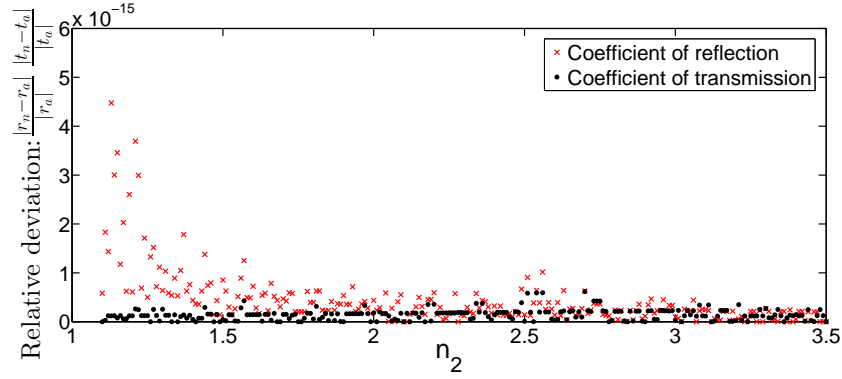
Figure 2.3 This graph shows the relative deviation between a single interface inter-action computed numerically (r_n and t_n) with MATLAB and analytically (r_a and t_a) at an incident light wavelength 633 nm with an amplitude of 1. The refractive index in the first domain is 1 and varied in the second domain between 1.1 and 4 for each data-point. It is seen that the precision is within the numerical range of MATLAB, which verifies that the code is functioning.

2.4 Fiber Bragg grating

Now that we have verified that the code is working we can try to apply it to an existing device. The fiber Bragg grating is a device used as a photonic filter, which filters light by reflecting specific wavelengths within a fiber.

It consists of a fiber which has a periodic or aperiodic small variation in refractive index. The grating can be manufactured with a laser by creating an interference-pattern within the fiber, changing the refractive indices of the fiber thus creating the grating.

In the following we will be examining a periodic grating and see an example of how the reflection of the Bragg-wavelength gets stronger as the length of the grating increases.

Given the following equations regarding the fiber Bragg grating for periods of the same length, we are able to specify a Bragg wavelength and a gap spanning over additional wavelengths in an interval around the Bragg wavelength. This gap is also known as a photonic band gap.

$$\omega_m = \frac{n_1 + n_2}{4 n_1 n_2} \tag{2.19}$$

$$\frac{\Delta\omega}{\omega_w} = \frac{4}{\pi} \arcsin\left(\frac{|n_1 - n_2|}{n_1 + n_2}\right) \tag{2.20}$$

$$\lambda_m = \frac{4a}{\frac{1}{n_1} + \frac{1}{n_2}} = \frac{4a\, n_1 n_2}{n_1 + n_2}. \tag{2.21}$$

Here ω_m is the mid-gap frequency, $\Delta\omega$ the frequency gap, λ_m the Bragg wave-length, a the length of the period (here the length of a single repetition of grating with refractive index n_1 plus the length of a single repetition of grating

with refractive index n_2). Equation (2.20) holds for infinite long quarter-wave stack gratings, which is not the case for the example we will be looking at, but can be used as a qualitative measure of the wavelengths through the grating [4].

We use our code to create a fiber Bragg grating with the following parameter values: $n_1 = 1.44$ $n_2 = 1.45$ we assume the wave propagates through air ($n = 1$) into a SiO_2 grating. By adjusting the amount of repetitions N over an interval of wavelengths from 1500 nm to 1600 nm we get a plot as shown in figure 2.4. It is seen that the amount of light transmitted through the fiber varies with the wavelength of the incoming light, we note at the wavelength 1555 nm the transmission decreases. As we increase N the frequency or wavelength gap becomes smaller more confined around the Bragg wavelength in tone with (2.20) which as stated holds for infinite long gratings.

We use the code to simulate a wave through this Bragg grating $N = 250$ at the wavelengths 1555 nm and 1520 nm. The resulting waves are sketched in figure 2.5 and we see just as we would expect from figure 2.4 that the total wave at $\lambda_0 = 1555$ nm experiences an overall reduction while the total wave at $\lambda_0 = 1520$ nm is not affected drastically.
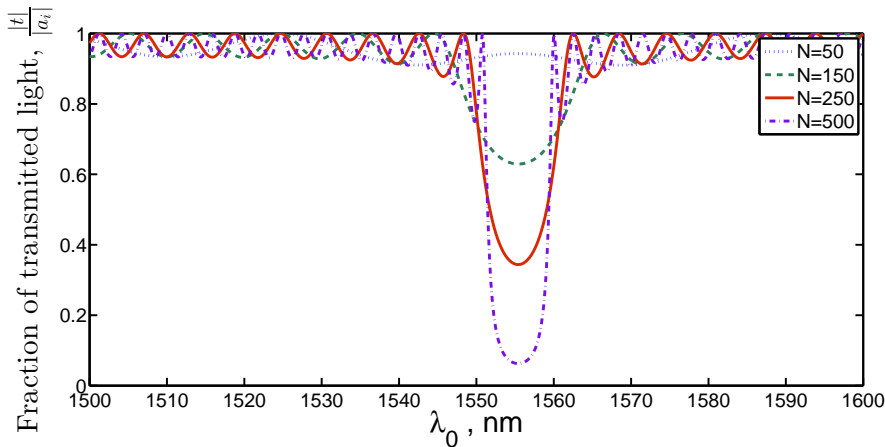
Figure 2.4 The fraction of transmitted light through a fiber Bragg grating structure versus different values for λ_0. Each graph represents different lengths of grating given by the number of times N a grating with periodic varying refractive indices $n_1 = 1.44$ and $n_2 = 1.45$ with an individual length of 269.1 nm is repeated. It is seen that the longer the grating is, the stronger the reflection of a given Bragg-wavelength becomes. In this case we get a strong reflection of the Bragg-wavelength 1555 nm.
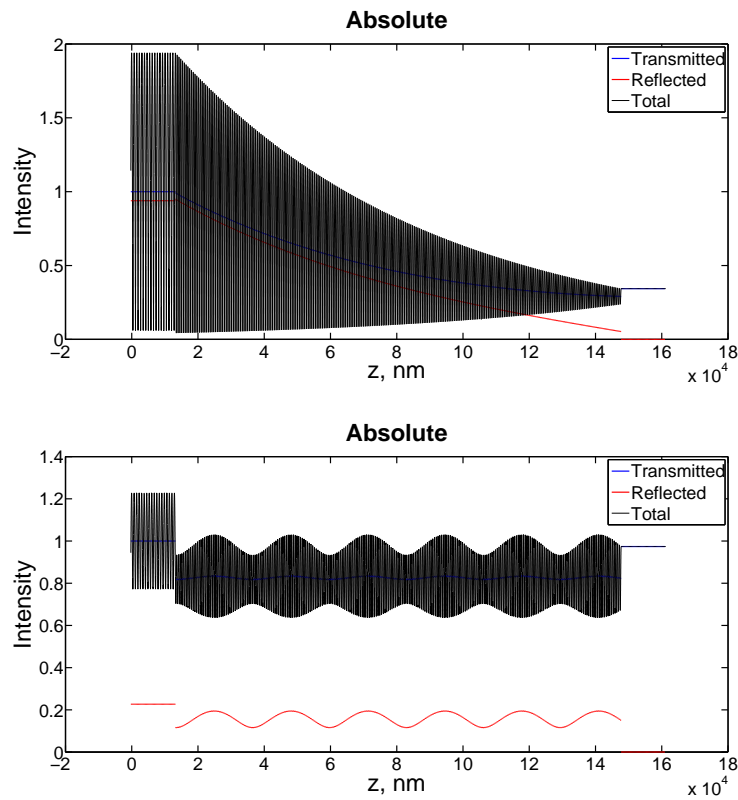
Figure 2.5 A fiber Bragg grating structure tested with our code using specifications $N = 250$ $n_1 = 1.44$ and $n_2 = 1.45$ with the length of each domain as 269.1 nm. The top graph shows a wave propagating through the grating at $\lambda_0 = 1555$ nm, here the transmittance decreases as expected from figure 2.4. The bottom graph shows a wave propagating through the grating at $\lambda_0 = 1520$ nm, here the transmittance do not decrease as much in accordance to what we would expect at this wavelength.

Volume integral equation in one dimension

3.1 Green's function

Until now we have determined the wave functions of the light using boundary conditions. To solve the problem more generally in a way that is easier to migrate to the corresponding three dimensional problem, we introduce the volume integral equation and solving this using Green's function. The idea is that we have a situation where there is a background media that has the same permittivity all the way through. In this background media we place some light scatters with a permittivity different from the background. The differential equation in (2.13) can be written as

$$\frac{\partial^2}{\partial z^2}E_x(z) + k_0^2\epsilon_B E_x(z) = -k_0^2\Delta\epsilon_r(r)E_x(z) \equiv -d(z), \qquad (3.1)$$

where $\Delta\epsilon_r(r) = \epsilon_r - \epsilon_B$, and ϵ_B is the permittivity of the background media. We notice that outside the scatters $\Delta\epsilon_r(r) = 0$ and the differential equation reduces to the belonging homogeneous equation. This rewriting of the differential equation is made because we need a term on the right side that is a so called drive term, a term that differs from point to point. By introducing the differential operator $L(f) = \frac{\partial^2}{\partial z^2}f + k_0^2\epsilon_B f$ we have $L(E(z)) = -d(z)$ and $L(E_0) = 0$. Generally the solution to $L(f)$ is given by $f = f_0 + f_p$ where f_0 is the complete solution to the homogeneous equation and f_p is a particular solution to the inhomogeneous equation. In terms of the electric field we have $E = E_0 + E_p$.

The Green's function is defined as the function $g(z, z')$ that solves: [5]

$$L(g) = \frac{\partial^2}{\partial z^2}g(z, z') + k_0^2\epsilon_B g(z, z') = -\delta(z - z'). \qquad (3.2)$$

Here $\delta(z - z')$ is the Dirac delta function. Our particular solution to the differential equation is then

$$f_p = \int g(z, z')d(z')dz', \qquad (3.3)$$

or in terms of the electric field

$$E_p = \int g(z, z') k_0^2 \Delta\epsilon_r(z') E_x(z') dz'. \tag{3.4}$$

The electric field is now

$$E_x(z) = E_{x,0}(z) + k_0^2 \int_{z_{scat}} g(z, z') \Delta\epsilon_r(z') E_x(z') dz'. \tag{3.5}$$

Here z_{scat} is the interval(s) of z where the light scatter is. This equation is quite complicated to solve because the unknown function, $E_x(z)$, is included implicitly due to the integration. When $E_x(z)$ is known inside the scatter, it can easily be found outside the scatter since the equation is now a explicit expression for $E_x(z)$.

To find the Green's function we solve (3.2), firstly for $z \neq z'$. Due to the Dirac delta function this gives a homogeneous equation that has the solution $g(z, z') = A\exp(ik_Bz) + B\exp(-ik_Bz)$. Using boundary conditions with a source at z' and an observation at z we must demand that the wave (Green's function) is forward travelling for $z > z'$ and backward travelling for $z < z'$. This gives us:

$$g(z, z') = \left\{ \begin{array}{c} A\exp(ik_Bz), z > z' \\ B\exp(-ik_Bz), z < z' \end{array} \right\}. \tag{3.6}$$

Also the function must be continuous at $z = z'$ which gives that $B = A\exp(2ik_Bz')$. By integrating (3.2) we get

$$\int_{z'-\varepsilon}^{z'+\varepsilon} \left[\frac{\partial^2}{\partial z^2} g(z, z') + k_0^2 \epsilon_B g(z, z') \right] dz = -\int_{z'-\varepsilon}^{z'+\varepsilon} \delta(z - z') dz, \quad \varepsilon \to 0 \Rightarrow \tag{3.7}$$

$$\frac{d}{dz} g(z, z') \mid_{z=z'+} - \frac{d}{dz} g(z, z') \mid_{z=z'-} = -1 \Rightarrow \tag{3.8}$$

$$A = \frac{i}{2k_B} \exp(-ik_Bz'). \tag{3.9}$$

Integrating over the continuous function $k_0^2 \epsilon_B g(z, z')$ and letting $\varepsilon \to 0$ gives zero, and the integral of the Dirac delta function results in 1. The Green's function is therefore

$$g(z, z') = \left\{ \begin{array}{c} \dfrac{i}{2k_B} \exp(ik_B(z - z')), z > z' \\ \dfrac{i}{2k_B} \exp(-ik_B(z - z')), z < z' \end{array} \right\}. \tag{3.10}$$

To use this we look at a system with one light scatter with permittivity ϵ_1 on a background media with permittivity ϵ_B. In (3.5) an expression for the field is inserted, $E_x(z) = A\exp(ik_1z) + B\exp(-ik_1z)$, which is a guess of how the form of the field expression is. This guess seems legit since we know that the field follows this form outside the scatters due to the inhomogenous differential equation belonging to (3.1). The challenge is then to determine the constants A and B. This is done by solving the equation separately for $z \in [z_0; z_1]$ and

for $z \notin [z_0; z_1]$ With $E_{x,0} = A_0 \exp(ik_B z)$ being a known wave to be sent in at the scatter the equation now gives

$$A \exp(ik_1 z) + B \exp(-ik_1 z) = A_0 \exp(ik_B z)$$
$$+ k_0^2 \int_{z_{scat}} g(z, z') \Delta \epsilon_r(z') A \exp(ik_1 z') dz'$$
$$+ k_0^2 \int_{z_{scat}} g(z, z') \Delta \epsilon_r(z') B \exp(-ik_1 z') dz'. \tag{3.11}$$

That is one equation with two unknown parameters, A and B. Two equations are created by multiplying with $\exp(ik_1 z)$ or $\exp(-ik_1 z)$. The two new equations are then integrated for $z_0 \leq z \leq z_1$ where $z_{0,1}$ is the boundaries of the scatterer, and this gives us two equations with two unknown parameters A, B which can easily be solved using matrix algebra. When the field is found inside the scatter we can easily determine the field outside the scatter since (3.5) is now a explicit expression of the field, which means the integration for z is unnecessary. To
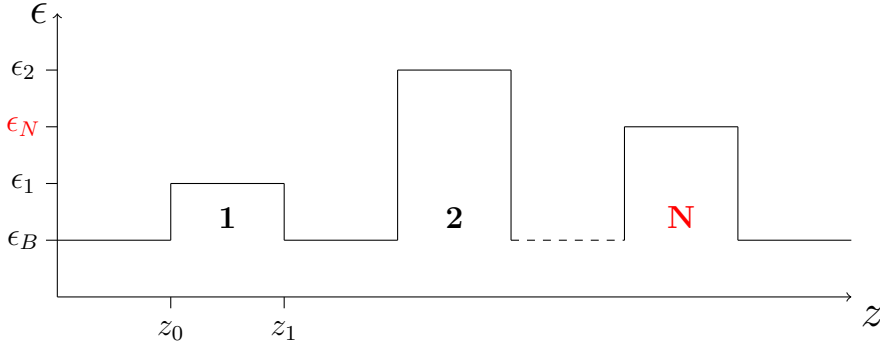

Figure 3.1 System consisting of N light scatters

expand this method to a system consisting of N scatters, as seen in figure 3.1, we introduce some notations that simplifies the equations. The basis function for the field is written as

$$e_{\alpha,J} = \frac{1}{\sqrt{L_J}} s_J(z) \exp\left((-1)^{\alpha+1} i k_J z\right), \tag{3.12}$$

where α has the value 1 for a forward travelling wave, and 2 for a backwards travelling wave. J is the number of the scatter. The function $S_J(z)$ has the following properties

$$S_J(z) = \left\{ \begin{matrix} 1, z \in z_J \\ 0, \text{otherwise} \end{matrix} \right\}.$$

Here z_J is the z-interval of the J'th scatter. The field inside the J'th scatter is now

$$E_J(z) = E_B(z) + k_0^2 \sum_{J'=1}^{N} \Delta \epsilon_{J'} \int_{J'} g(z, z') E_J'(z') dz', \tag{3.13}$$

where $E_J = A_J e_{1,J} + B_J e_{2,J}$. The idea is the same; we generate $2N$ equations by multiplying this equation with all the different basis functions $e^*_{\alpha,J}$ (* denotes a complex conjugation). The equations can be written as a matrix system

$$\mathbf{Mx} = \mathbf{M}_B\mathbf{x}_B + k_0^2\boldsymbol{\Delta\epsilon}\mathbf{Gx}, \tag{3.14}$$

where $\mathbf{x}$ consists of all the unknown coefficients $A_1, B_1, ..., A_N, B_N$ and $\mathbf{x}_B$ consists of the known coefficients of the incoming light. The different matrices can be computed systematic by introducing bra-ket notations since they will appear a lot in the equations.

$$< e_{\alpha,J}|e_{\alpha',J'} > \equiv \int_{-\infty}^{\infty} e^*_{\alpha,J}(z)e_{\alpha',J'}(z)dz, \tag{3.15}$$

$$< e_{\alpha,J}|e^B_{\alpha',J'} > \equiv \int_{-\infty}^{\infty} e^*_{\alpha,J}(z)e^B_{\alpha',J'}(z)dz, \tag{3.16}$$

$$< e_{\alpha,J}|g|e_{\alpha',J'} > \equiv \int_{L_J} e^*_{\alpha,J}(z)\left[\int_{L_{J'}} g(z,z')e_{\alpha',J'}(z)dz'\right]dz. \tag{3.17}$$

The matrices and the bra-ket expression can be seen in appendix B. This kind of matrix equation can easily be solved numerically using MATLAB backslash command.

3.2 Silver particles as light scatters

In order to relate these one-dimensional methods to our main article we will look at an example of three light scatters. This should compare to the first example in the article with three silver particles in a line array where the particles are illuminated with a $0°$ or $180°$ angle. The purpose is to see if we can achieve high intensity of light around one (or two) of the scatters while low intensity at the rest.

To simulate the metal scatters we introduce a complex refractive index. This results in a damping of the light through the metal due the imaginary part of the index. To calculate the refractive indices of the simulated particles we use the Drude model that relates the permittivity of metal to the cyclic frequency of light: [6]

$$\epsilon_{metal}(\omega) = 1 - \frac{\omega_p^2}{\omega^2 + i\gamma\omega}, \tag{3.18}$$

where ω_p is the plasma frequency and γ is the collision frequency. The refractive index is related to the permittivity as $n = \sqrt{\epsilon}$. For silver the following parameters are used:

$$\omega_p^{Ag} = 1.2 \cdot 10^{16}\mathrm{s}^{-1}, \tag{3.19}$$

$$\gamma^{Ag} = 9.1 \cdot 10^{13}\mathrm{s}^{-1}. \tag{3.20}$$

Using these parameters the refractive index of the silver particles is:

$$n = 0.41 + 3.02i, \tag{3.21}$$

for a wavelength of 500 nm.

Using the refractive index calculated with the Drude model, a wavelength of 500 nm, a scatter size of 50 nm separated by 150 nm we achieve the results shown in figure 3.2 where the silver is highlighted with grey scaling.
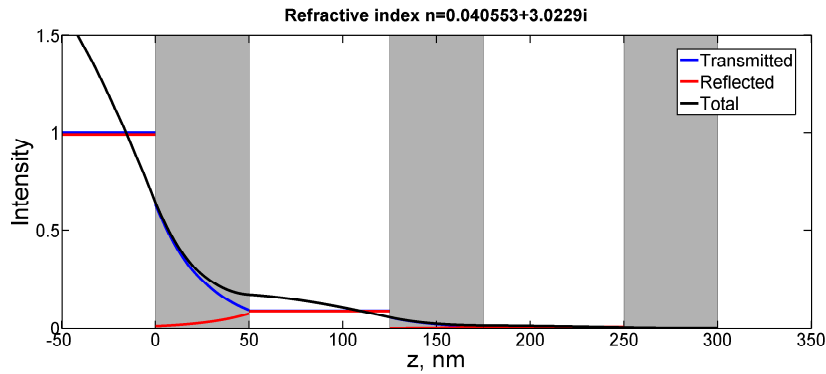

Figure 3.2 Three silver scatters illuminated with a light of 500 nm. The scatter size is 50 nm and the separation distance is 75 nm.

In the article by Koenderink et al. the sphere farthest away from the light is illuminated. In figure 3.2 we see that the intensity is highest around the scatter closest to the incoming light and lower around the others. Though the intensity is higher around one scatter we cant recognize the same effects as for the three-dimensional simulation discussed in the article and we must conclude that our code cannot be used to simulate nanolithography.

Though the main purpose with this example was not fulfilled there are still interesting things about the figure. The effect of the imaginary part of the refractive index is clearly shown in the graph. We see that the transmitted (blue) light is damped in the forward travelling direction while the reflected (red) is damped in the other direction.

Three-dimensional simulations

4.1 Introduction

By now we have investigated how light interferes with media with different permittivity in one dimension. We have done this using two different methods; a simple method using boundary conditions at each interface and a more complex method using the volume integral equation in one dimension. In three dimensions we need to look at the three-dimensional version of the volume integral equation as seen in (4.1): [7]

$$\mathbf{E}(\mathbf{r}) = \mathbf{E}_B(\mathbf{r}) + k_0^2 \int_{V_{scat}} \mathbf{G}_B(\mathbf{r}, \mathbf{r}')\Delta\epsilon(\mathbf{r}')\mathbf{E}(\mathbf{r}')d\mathbf{r}'. \tag{4.1}$$

The difference to the one-dimensional version is that the electric field here is an actual field with three components instead of just the one. Also the Green's function transforms to a Green's tensor in the 3D equation. The methods used to solve the 3D equation is parallel to those used for 1D, but actually doing it must wait a couple of years. Instead we will use the MATLAB code developed by J.R. de Lasson to simulate our examples.

4.2 Simulation of three particles in line array

As presented in the article by Koenderink et al. we will look at a system consisting of three silver particles in a line array. As mentioned in the introduction they achieve some quite impressive results when they light spheres of radii 25 nm and distance 75 nm with light of 500 nm wavelength and then scanning over an angle from 0° to 180°.

Using the mentioned code and the same parameters as in the article we get the results presented in figure 4.1. The equivalent field plot a distance of 5 nm above the spheres for an angle of 0° and 90° is presented in figure 4.2a and 4.2b. We notice that we don't achieve the same results as in the Koenderink article where one sphere was exposed with a high contrast for an angle of 0 or 180 degrees. We get that 2 spheres are approximately equally exposed but not with a contrast that is anywhere near the contrasts in the article. There is one qualitative equality between our simulation and the article, and that is the light is gathered farthest away from the incoming light. Logically you might say that
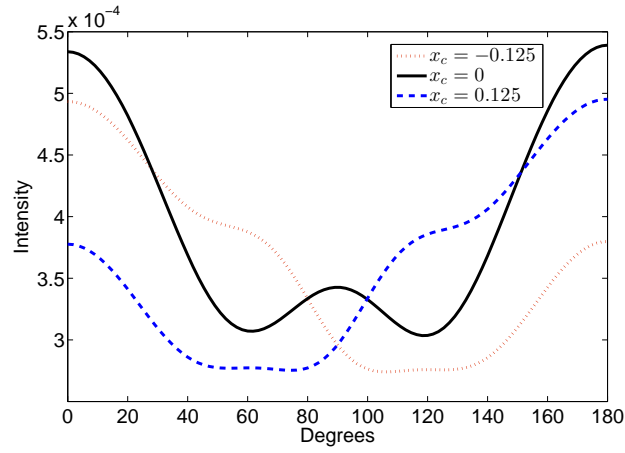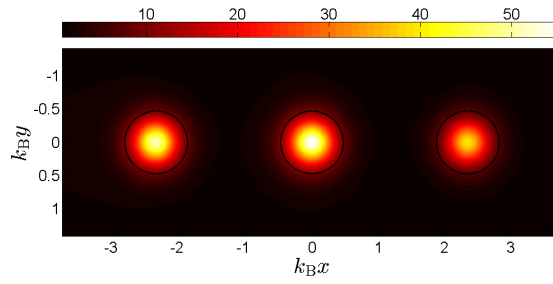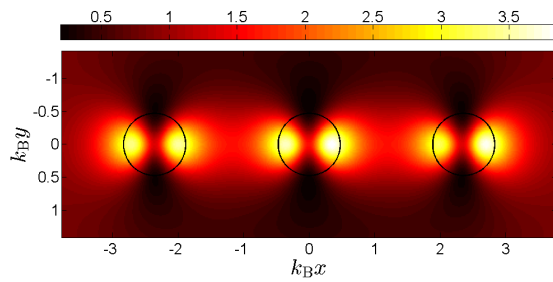
Figure 4.1 Plot of intensity versus angle in degrees

(a) Angle 0 degrees

(b) Angle 90 degrees

Figure 4.2 Field plot a distance of 5 nm above the spheres for various angles

the sphere closest to the incoming light should be exposed the most but due to
the complex plasmon interferences we see that it is actually the spheres farthest

away from the incoming light that is exposed the most.

One of the reasons that our results don't match with the article could be that Koenderink et al. uses a point dipole model, which is an approximation of the field inside the metal spheres. It states that the field is constant over the volume of the spheres since the spheres are small compared to the wavelength of the field. To investigate this approximation we plot the field in a plane through the center of the spheres for an angle of 0 degrees.

As seen in figure 4.3, especially for the sphere in the middle, the approximation of the field being constant through the sphere might be a rough approximation. Using the bar above the figure the intensity is about 7 in the center and about 10 at the edge of the sphere. This is a quite big difference and therefore it questions the validity of the approximation and thereby the results achieved by Koenderink et al. [1].
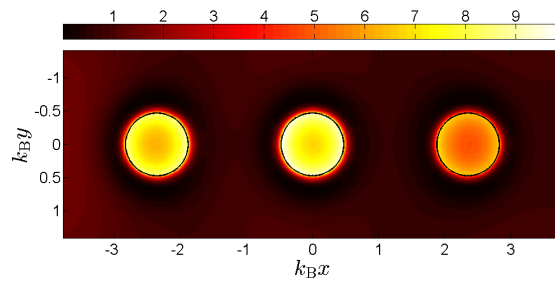

Figure 4.3 Field plot through center of the spheres with a wavelength of 500 nm and angle of incoming light 0 degrees

Discussion

If we despite the fact that our results has been conflicting the findings of Koenderink et al. [1], pretended that it was actually possible to create a mask using spherical silver particles we still see some major challenges in order to implement this into practical applications.

To begin with a person will need to design a proper photoresist responsive to the power dissipated from the spheres, as stated by an expert in the field of micro- and nanofabrication E. V. Thomsen, professor at DTU Nanotech. The resist cannot be exposed by the light we use to illuminate the silver particles since the mask array of particles is underneath the resist. Also the resist needs to have the right contrast specifications that match those of the field produced by the particles.

If we have the proper resist a new problem arises - the placement of the particles. One does not simply place tiny silver particles in an array with such a great precision. If high precision is necessary we would need a way to place the particles and a technique to keep them in place. For that purpose we could design a material that works self calibrating, where the lattice structure of the material helps aligning the silver particles in the desired pattern. Another problem occurs when we want to apply photoresist to the mask. The process is usually done by spin coating, meaning the mask is rotated at a high velocity under the application of photoresist, which undoubtedly would displace the particles.

Even if we assume that you created a resist, there are still difficulties that have to be considered. When we have finished the exposure process and created our desired pattern we need to separate the photoresist from the mask - a lift off process. Usually in fabrication of nanostructures the photoresist act as a mask and is already in place on top of a substrate, however in our case we want to move our resist to another substrate, meaning we would have to develop a way to move the photoresist from the particle mask to a substrate where it is going to be used.

To sum up we are experiencing multiple problems and challenges with the practical applications of programmable nanolithography as well as the theoretical discrepancy of the results achieved by Koenderink et al.

Conclusion

In power of the research done in this paper we are hereby able to conclude the following.

We started by looking at the problem of light scattering in one dimension. A MATLAB program was developed to simulate wave interactions in one dimension. This program was used to investigate whether the effects of gathering light around light scatters were possible. The conclusion to this was that we did not see these effects in one dimension due to missing plasmon effects. This led us to the similar problem in three dimensions which was examined using a MATLAB program based on the three dimensional volume integral equation. The results achieved using this program was inconsistent with the results presented by Koenderink et al. Qualitatively we saw some of the same phenomena, though the contrasts of the patterns were insufficient compared to those in the article [1]. The differences between our results and theirs were discussed, taking the approximation using the point dipole model into consideration.

Leaving the theoretical challenges for a while, we have discussed the problems of an actual practical application using a top-down approach. The problems of the different processes were discussed chronologically and plausible solutions were considered.

The overall purpose of the project was to prove the possibility of programmable nanolithography. We have come to the conclusion that we cannot validate the outcome of the article and an invalidation of programmable nanolithography as a whole cannot be made without taking an experimental approach to the problem.

Matrices with boundary conditions

This is the generated matrix from section 2.3 example with 3 interfaces.

$$
M =
\begin{bmatrix}
\exp(-ik_1z_1) & -\exp(ik_2z_1) & -\exp(-ik_2z_1) & 0 & 0 & 0 \\
-k_1\exp(-ik_1z_1) & -k_2\exp(ik_2z_1) & k_2\exp(-ik_2z_1) & 0 & 0 & 0 \\
0 & \exp(ik_2z_2) & \exp(-ik_2z_2) & -\exp(ik_3z_2) & -\exp(-ik_3z_2) & 0 \\
0 & k_2\exp(ik_2z_2) & -k_2\exp(-ik_2z_2) & -k_3\exp(ik_3z_2) & k_3\exp(-ik_3z_2) & 0 \\
0 & 0 & 0 & \exp(ik_3z_3) & \exp(-ik_3z_3) & -\exp(ik_4z_3) \\
0 & 0 & 0 & k_3\exp(ik_3z_3) & -k_3\exp(-ik_3z_3) & -k_4\exp(ik_4z_3)
\end{bmatrix}
$$

$$
c =
\begin{bmatrix}
-A_I\exp(ik_1z_1) \\
-k_1\,A_I\exp(ik_1z_1) \\
0 \\
0 \\
0 \\
0
\end{bmatrix}
$$

Matrices with Green's function

The matrices in the matrix equation (3.14) can be expressed as

$$
\mathbf{M} = \begin{bmatrix}
< e_{1,1}|e_{1,1} > & < e_{1,1}|e_{2,1} > & 0 & 0 & \cdots & 0 & 0 \\
< e_{2,1}|e_{1,1} > & < e_{2,1}|e_{2,1} > & 0 & 0 & \cdots & 0 & 0 \\
0 & 0 & < e_{1,2}|e_{1,2} > & < e_{1,2}|e_{2,2} > & \cdots & 0 & 0 \\
0 & 0 & < e_{2,2}|e_{1,2} > & < e_{2,2}|e_{2,2} > & \cdots & 0 & 0 \\
\vdots & \vdots & \vdots & \vdots & \ddots & \vdots & \vdots \\
0 & 0 & 0 & 0 & \cdots & < e_{1,N}|e_{1,N} > & < e_{1,N}|e_{2,N} > \\
0 & 0 & 0 & 0 & \cdots & < e_{2,N}|e_{1,N} > & < e_{2,N}|e_{2,N} >
\end{bmatrix}
\tag{B.1}
$$

$$
\mathbf{M}_B = \begin{bmatrix}
< e_{1,1}|e_{1,1}^B > & < e_{1,1}|e_{2,1}^B > \\
< e_{2,1}|e_{1,1}^B > & < e_{2,1}|e_{2,1}^B > \\
< e_{1,2}|e_{1,2}^B > & < e_{1,2}|e_{2,2}^B > \\
< e_{2,2}|e_{1,2}^B > & < e_{2,2}|e_{2,2}^B > \\
\vdots & \vdots \\
< e_{1,N}|e_{1,N}^B > & < e_{1,N}|e_{2,N}^B > \\
< e_{2,N}|e_{1,N}^B > & < e_{2,N}|e_{2,N}^B >
\end{bmatrix}
\tag{B.2}
$$

$$
\mathbf{x} = \begin{bmatrix}
A_1 \\
B_1 \\
A_2 \\
B_2 \\
\vdots \\
A_N \\
B_N
\end{bmatrix}
\tag{B.3}
$$

$$\mathbf{G} = \begin{bmatrix}
\langle e_{1,1}|g|e_{1,1}\rangle & \langle e_{1,1}|g|e_{2,1}\rangle & \langle e_{1,1}|g|e_{1,2}\rangle & \langle e_{1,1}|g|e_{2,2}\rangle & \cdots & \langle e_{1,1}|g|e_{1,N}\rangle & \langle e_{1,1}|g|e_{2,N}\rangle \\
\langle e_{2,1}|g|e_{1,1}\rangle & \langle e_{2,1}|g|e_{2,1}\rangle & \langle e_{2,1}|g|e_{1,2}\rangle & \langle e_{2,1}|g|e_{2,2}\rangle & \cdots & \langle e_{2,1}|g|e_{1,N}\rangle & \langle e_{2,1}|g|e_{2,N}\rangle \\
\langle e_{1,2}|g|e_{1,1}\rangle & \langle e_{1,2}|g|e_{2,1}\rangle & \langle e_{1,2}|g|e_{1,2}\rangle & \langle e_{1,2}|g|e_{2,2}\rangle & \cdots & \langle e_{1,2}|g|e_{1,N}\rangle & \langle e_{1,2}|g|e_{2,N}\rangle \\
\langle e_{2,2}|g|e_{1,1}\rangle & \langle e_{2,2}|g|e_{2,1}\rangle & \langle e_{2,2}|g|e_{1,2}\rangle & \langle e_{2,2}|g|e_{2,2}\rangle & \cdots & \langle e_{2,2}|g|e_{1,N}\rangle & \langle e_{2,2}|g|e_{2,N}\rangle \\
\vdots & \vdots & \vdots & \vdots & \ddots & \vdots & \vdots \\
\langle e_{1,N}|g|e_{1,1}\rangle & \langle e_{1,N}|g|e_{2,1}\rangle & \langle e_{1,N}|g|e_{1,2}\rangle & \langle e_{1,N}|g|e_{2,2}\rangle & \cdots & \langle e_{1,N}|g|e_{1,N}\rangle & \langle e_{1,N}|g|e_{2,N}\rangle \\
\langle e_{2,N}|g|e_{1,1}\rangle & \langle e_{2,N}|g|e_{2,1}\rangle & \langle e_{2,N}|g|e_{1,2}\rangle & \langle e_{2,N}|g|e_{2,2}\rangle & \cdots & \langle e_{2,N}|g|e_{1,N}\rangle & \langle e_{2,N}|g|e_{2,N}\rangle
\end{bmatrix} \tag{B.4}$$

where the following bra-ket notations are used:

$$< e_{\alpha,J}|e_{\alpha',J'}> \equiv \int_{-\infty}^{\infty} e_{\alpha,J}^*(z)e_{\alpha',J'}(z)dz \tag{B.5}$$

$$= 0 \text{ for } J \neq J' \tag{B.6}$$

$$= 1 \text{ for } J = J' \text{ and } \alpha = \alpha' \tag{B.7}$$

$$= \frac{1}{L_J}\frac{i}{2k_J}\left(\exp(-2ik_J z_{1,J}) - \exp(-2ik_J z_{0,J})\right) \text{ for } J = J' \text{ and } \alpha \neq \alpha' \tag{B.8}$$

$$< e_{\alpha,J}|e_{\alpha',J'}^B> \equiv \int_{-\infty}^{\infty} e_{\alpha,J}^*(z)e_{\alpha',J'}^B(z)dz \tag{B.9}$$

$$= 0 \text{ for } J \neq J' \tag{B.10}$$

$$= \frac{1}{L_J}\frac{1}{i(k_B - k_J)}\left(\exp(i(k_B - k_J)z_{1,J}) - \exp(i(k_B - k_J)z_{0,J})\right) \text{ for } J = J' \text{ and } \alpha = \alpha' = 1 \tag{B.11}$$

$$= \frac{1}{L_J}\frac{-1}{i(k_B - k_J)}\left(\exp(-i(k_B + k_J)z_{1,J}) - \exp(-i(k_B + k_J)z_{0,J})\right) \text{ for } J = J' \text{ and } \alpha = 1, \alpha' = 2 \tag{B.12}$$

$$= \frac{1}{L_J}\frac{1}{i(k_B - k_J)}\left(\exp(i(k_B + k_J)z_{1,J}) - \exp(i(k_B + k_J)z_{0,J})\right) \text{ for } J = J' \text{ and } \alpha = 2, \alpha' = 1 \tag{B.13}$$

$$= \frac{1}{L_J}\frac{1}{i(k_J - k_B)}\left(\exp(i(k_J - k_B)z_{1,J}) - \exp(i(k_J - k_B)z_{0,J})\right) \text{ for } J = J' \text{ and } \alpha = 2, \alpha' = 1 \tag{B.14}$$

$$< e_{\alpha,J}|g|e_{\alpha',J'}> \equiv \int_{L_J} e_{\alpha,J}^*(z)\left[\int_{L_{J'}} g(z,z')e_{\alpha',J'}(z)dz'\right]dz \tag{B.15}$$

Bibliography

[1] A. F. Koenderink, J. V. Hernández, F. Robicheaux, L. D. Noordam, and A. Polman, "Programmable nanolithography with plasmon nanoparticle arrays," Nano Letters **7**, 745–749 (2007).

[2] D. Griffiths, *Introduction to Electrodynamics*, Pearson international edition (Pearson Education, Limited, 2012).

[3] MathWorks, "`http://www.mathworks.se/help/matlab/matlab_prog/floating-point-numbers.html`," (2014).

[4] J. Joannopoulos, S. Johnson, J. Winn, and R. Meade, *Photonic Crystals: Molding the Flow of Light (Second Edition)* (Princeton University Press, 2011).

[5] Wikipedia, "`en.wikipedia.org/wiki/Green's_function`," (2014).

[6] J. R. de Lasson, "Electromagnetic scattering in micro- and nanostructured materials," Master's thesis, Technical University of Denmark (2012).

[7] J. R. de Lasson, J. Mørk, and P. T. Kristensen, "Three-dimensional integral equation approach to light scattering, extinction cross sections, local density of states, and quasi-normal modes," J. Opt. Soc. Am. B **30**, 1996–2007 (2013).